Laboratory studies of X-ray emission from Fe L-shell transitions and their diagnostic utility

G.V. Brown[*], P. Beiersdorfer[*], H. Chen[*], J. H. Scofield[*], K. R. Boyce,[†], R. L. Kelley[†], C. A. Kilbourne[†], F. S. Porter[†], N. S. Brickhouse[**], M. F. Gu[‡], S. M. Kahn[‡] and A. E. Szymkowiak[§]

[*]*Lawrence Livermore National Laboratory, 7000 East Avenue, Livermore, CA 94550*
[†]*NASA/Goddard Space Flight Center, Greenbelt, MD, 20771*
[**]*Harvard-Smithsonian Center for Astrophysics, 60 Garden Street, Cambridge, MA 02138*
[‡]*Department of Physics, Stanford University, Stanford, CA 94305*
[§]*Department of Physics, Yale University, New Haven, CT 06520*

Abstract. Celestial objects are often home to complex, dynamic, intriguing environments. High-resolution x-ray spectra from these sources measured by satellites such as the *Chandra*, *XMM-Newton*, the *Solar Maximum Mission*, and the soon-to-be-launched *Astro-E2* provide a means for understanding the physics governing these sources. Especially rich is the x-ray emission from L-shell transitions in highly charged iron ions. This emission is the source of a variety of diagnostics whose utility lies in the accuracy of the atomic data employed to model the x-ray spectra. The atomic data used to describe these diagnostics are generally provided by large theoretical calculations and benchmarked by laboratory data. In this paper we discuss laboratory measurements of Fe L-shell x-ray emission including wavelengths, relative and absolute excitation cross sections, and line ratios that provide diagnostics of temperature and density.

INTRODUCTION

Beginning in the mid 1960s, spectrometers carried by sounding rockets and orbiting satellites have measured high-resolution spectra from the Sun covering the 10–20 Å bandwidth [1, 2, 3, 4, 5, 6, 7]. From these measurements it was realized that the strong emission from Fe L-shell ions contains great diagnostic potential. With the successful launches of the *Chandra* and *XMM-Newton* X-ray observatories, high-resolution spectra of Fe L-shell emission are now routinely measured from a variety of extra-solar sources with the hope of taking full advantage of the diagnostics associated with the Fe L-shell ions. Reliable interpretation of spectra from solar and extra-solar sources requires accurate and complete databases of transition wavelengths and line strengths. Many improvements in spectral modeling packages used by the astrophysics community have been made such as the inclusion of large sets of recently available experimental data where available, and by utilizing experimentally benchmarked atomic theories to provide data when experimental results do not exist. In some cases, the inclusion of experimental data has made reliable interpretation of high-resolution spectra possible for the first time. Fe L-shell experimental data has been produced by several experimental facilities including storage rings (see Savin et al. these proceedings), tokamaks [8, 9], and electron beam ion traps [10]. Here we give a brief review of the laboratory astrophysics studies being conducted in the study of Fe L-shell x-ray emission at the LLNL EBIT facility.

CP774, *X-Ray Diagnostics of Astrophysical Plasmas,* edited by Randall K. Smith

WAVELENGTHS AND LINE IDENTIFICATION

Accurate line identification of observed emission is the first step towards understanding a spectrum and its source. In the past, the identification of Fe L-shell x-ray lines has proceeded by comparing calculated wavelengths and line intensities to experimental data from solar observations [4, 5, 6, 11] and emission from tokamak and laser produced plasmas [9, 12]. Problems arise because these experimental sources all emit x-rays from several different Fe ions simultaneously. This limits the number of lines that can be identified and the accuracy of the wavelengths that can be measured because lines from different charge states blend even when measured with high-resolution spectrometers. In spite of these challenges, several databases of line intensities and wavelengths have been compiled [13, 14, 15]. For these databases, calculations are used to provide wavelengths and line intensities where no experimental value exists.

In anticipation of the launch of the high-resolution instruments on board *Chandra* and *XMM-Newton* and to address problems found in the interpretation of *ASCA* data, all the line emission from Fe XVII–XXIV was measured using the LLNL electron beam ion traps (EBITs) [16, 17]. Because the electron beam on an EBIT is mono-energetic, we are able to produce and trap a single ionic species of Fe and measure its x-ray emission. This eliminates the spectral confusion among lines from different charge states. The wavelength of each transition is determined by comparing to well-known wavelengths of x-ray emission from hydrogenic and helium-like ions. Figure 1 shows the Rydberg series of helium-like O VII and two iron spectra. One iron spectrum was measured above the ionization potential of Fe^{16+} and one below. Above the ionization potential, the Fe XVIII line F1 is produced [18]. Thus, by changing the electron beam energy from above and below ionization potentials of different iron ions, line emission can be positively identified with a specific charge state. Once the charge state and wavelength are known, identification of each x-ray line was completed by comparing measured spectrum to a spectrum calculated by HULLAC. The wavelengths measured at the LLNL EBIT have been implemented in the Atomic Plasma Emission Code (APEC) making reliable line identifications of many lines measured by *Chandra* and *XMM-Newton* possible, and are being used to benchmark more recent calculations.

The wavelengths and line identifications provided by our experiments not only make possible the diagnostic utility of Fe L-shell transitions, but also increase the reliability of the diagnostics of other ionic species. For example, emission from helium-like neon, magnesium, and hydrogenic oxygen and neon also fall in the same wavelength band as the Fe L-shell lines. Without properly accounting for each iron line, the temperature and density diagnostics of each of these ions is precluded. Figure 2 shows a *Chandra* spectrum of Capella emphasizing the wavelength region around the Ne IX triplet. This spectrum shows that the Fe L-shell emission must be accounted for when using the Ne IX emission as a diagnostic.

THE RELATIVE INTENSITY OF THE FE XVII LINES 3C AND 3D

Two of the more distinct lines found in spectra of Fe L-shell emission are the resonance and intercombination lines from Fe XVII, known as 3C and 3D respectively. These lines

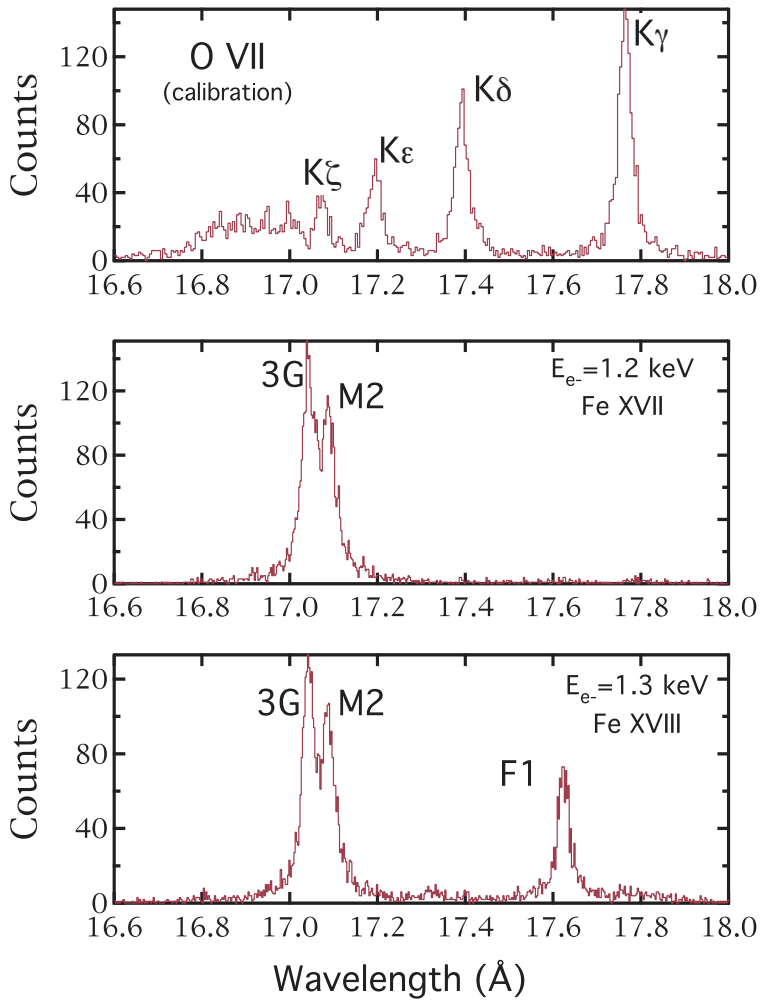

FIGURE 1. (top) Spectrum of helium-like O^{6+} x-ray emission used for calibration. (middle) Fe XVII spectrum taken at an electron beam energy of 1.2 keV. (bottom) Fe XVIII spectrum measured at an electron beam energy of 1.3 keV. The wavelength scale is determined by the line emission from O^{6+} and the lines are identified of the Fe L-shell emission are determined by comparing spectrum measured at different beam energies. These spectra demonstrate the utility of a mono-energetic electron beam in the identification of x-ray line emission. This figure is from [18].

are a result of the transitions $2p^5 3d_{3/2}\ ^1P_1$ and $2p^5 3d_{5/2}\ ^3D_1$ to the $2p^6\ ^1S_0$ ground state, and are located at 15.01 and 15.25 Å, respectively. They have been observed in observations of the Solar corona [1, 7, 3] and from other extra-solar sources [20, 21]. Owing to their prevalence, these lines have been a topic of studies for several decades. Comparison of the observed relative intensity I_{3C}/I_{3D} and the relative intensity calculated

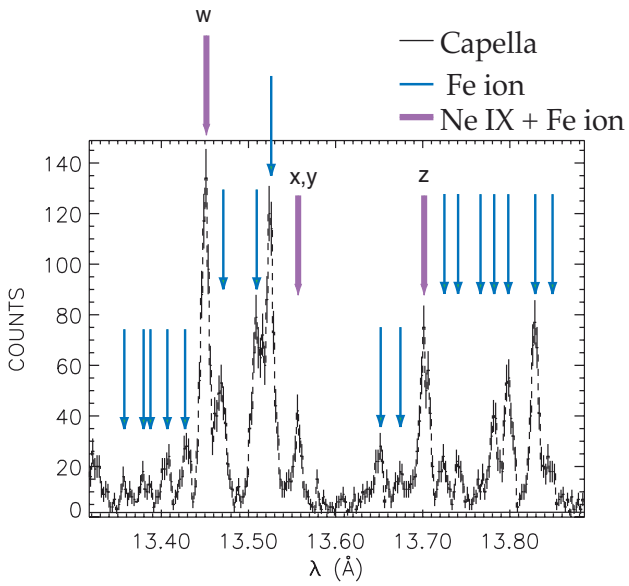

FIGURE 2. Spectrum of Capella depicting the region around the helium-like Ne^{8+} triplet. Several emission lines from Fe L-shell ions are present in this wavelength region and some blend with the lines w, x, y, and z of Ne^{8+}. Without accounting for all the iron emission, the accuracy of the temperature and density diagnostics associated with Ne IX is limited. This data can be found in [19].

by modern atomic codes shows that the calculation generally predict values significantly higher than observed. To account for the difference, some concluded that the emission from 3C is resonantly scattered out of the line of sight, reducing the relative intensity of I_{3C}/I_{3D} compared to the optically thin case. The reduced ratio I_{3C}/I_{3D} was then used to infer the optical depth of line 3C and the column density of the source [22]. However, because of the large variation among theoretical values for the optically thin ratio, correctly estimating the optical depth of 3C or the column density of the source was not possible.

To benchmark the relative intensity of I_{3C}/I_{3D} in the optically thin limit, it was measured at the LLNL EBIT [16]. Our results show the ratio to be 3 while most modern atomic codes predict values that are more than 20 % larger. Using our measured ratio and the methods given in Waljeski et al. [22], we derived the optical depth of line 3C as a function of I_{3C}/I_{3D}. Figure 3 shows a plot of τ(3C) versus I_{3C}/I_{3D} and compares the curve derived from our experimental ratio with different calculated optically thin ratios.

Although the measured value of $I_{3C}/I_{3D} = 3.04 \pm 0.12$ is significantly lower than many of the calculations, it is still not as low as some values measured in the corona of the Sun. To address the cause for these low ratios, we used the LLNL EBIT to measure the line ratio under conditions where a significant amount of Na-like Fe^{15+} was present at the same time as neon-like Fe^{16+} [23]. Figure 4 shows three spectra measured at the LLNL EBIT each with different relative abundances of Fe^{15+}/Fe^{16+}. In the top spectrum, the relative abundance is about 15%, in the middle spectrum 50 %, and in the bottom spectrum no Fe^{15+} is present. Our results show the presence of several Fe^{15+} x-ray lines in this wavelength band and that one of these lines coincides with the line 3D.

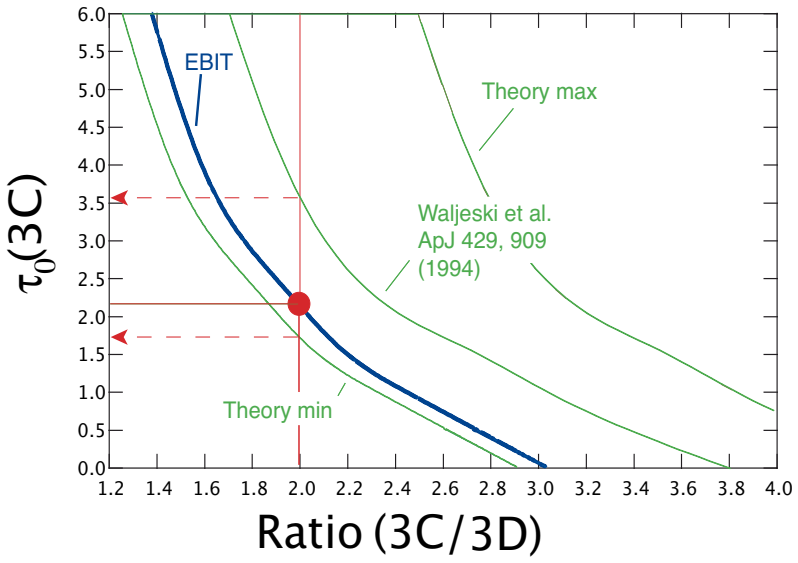

FIGURE 3. Plot of optical depth of the resonance line 3C versus intensity ratio 3C/3D. This figure compares the curve obtained using the experimental ratio to those obtained from different calculations.

Thus, when a significant amount of Fe^{15+} is present the ratio of I_{3C}/I_{3D} is reduced. The influence of Fe^{15+} innershell satellites was also pointed out by Behar, Cottam & Kahn [20] in their analysis of the high resolution spectrum of Capella provided by *Chandra*, and these line were tentatively identified by Phillips et al. in their analysis of solar spectra [7]. Also, the lower ratio measured from tokamak measurements provided by Beiersdorfer et al. [8] is consistent with our result.

The fact that an Fe^{15+} innershell satellite line increases the apparent strength of line 3D means I_{3C}/I_{3D} depends on the relative abundance of Fe^{15+} to Fe^{16+} and is, therefore, a function of temperature. Using the abundance versus temperature tables of Arnaud & Raymond [24], we plot the ratio I_{3C}/I_{3D} as a function of temperature in figure 5. Using the observed values of I_{3C}/I_{3D}, we also infer the temperature of Capella and of flaring and non-flaring active regions of the Sun.

EXCITATION CROSS SECTIONS

Although our laboratory measurements have provided a benchmark for the optically thin ratio of 3C/3D and demonstrated that the ratio can be reduced by an Fe $^{15+}$ innershell satellite that coincides with line 3D, the measurements of the relative intensity cannot point out if calculations predict the incorrect cross section for 3C, 3D, or both. To uncover the source of the problem, we have used the X-ray microcalorimeter built by the Goddard Space Flight Center/University of Wisconson X-ray microcalorimeter group and implemented at the LLNL EBIT facility [25, 26, 27] to measure the absolute cross section of both lines 3C and 3D [28]. Our method is the same as described in [29]. In brief, we take advantage of the fact the NASA/GSFC calorimeters have a

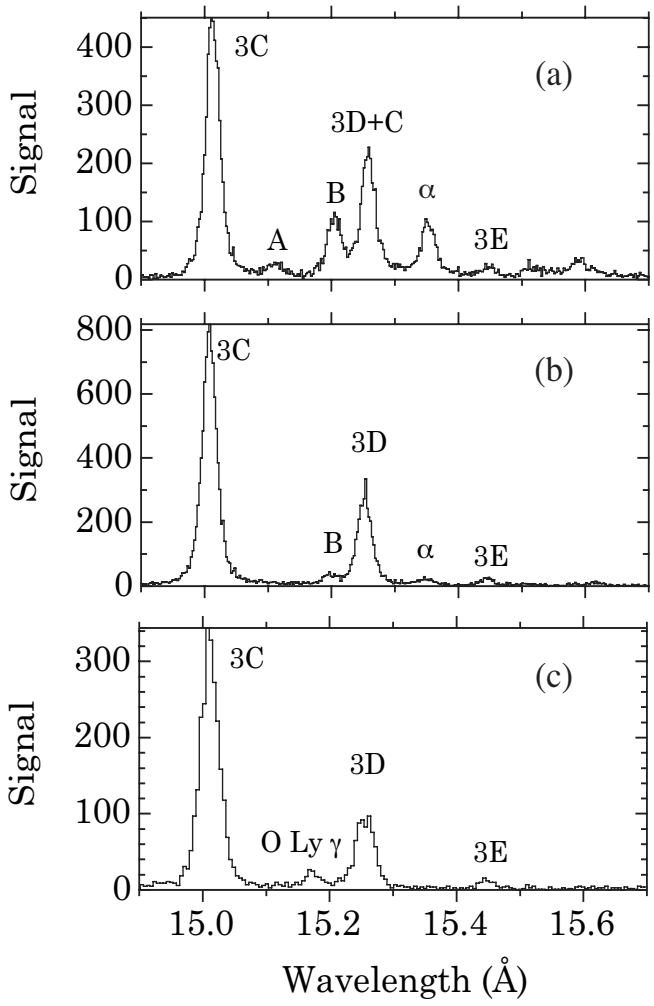

FIGURE 4. Comparison of Fe XVII spectra measured with different relative abundances of Fe^{15+} to Fe^{16+}. (a) $Fe^{15+}/Fe^{16+} \approx 1$. (b) $Fe^{15+}/Fe^{16+} \approx 0.15$. (c) $Fe^{15+}/Fe^{16+} = 0$. Lines 3C, 3D, and 3E are from Fe^{16+}, lines A, B, and C are from Fe^{15+}, and line α is from Fe^{14+}. This figure is from [23].

large bandwidth, long-time gain stability, a large collecting area, and relatively high resolution to simultaneously measure the emission from direct excitation and radiative recombination. Once both DE and RR emission are measured, we normalize our entire spectrum to the well-known cross sections of RR. In the case of Fe XVII, our results show that modern atomic theories predict cross sections for the resonance line 3C to be too large, while correctly predicting the cross section for the intercombination line 3D. This result not only provides the reason modern theories predict I_{3C}/I_{3D} to be too large, but also demonstrates the reason calculations underestimate the relative intensity of the $2p - 3s$ Fe XVII lines located around 17 Å relative to line 3C [30, 31]. Our result thus reduces the source of two long standing puzzles in the study of Fe XVII x-ray emission to a single emission line.

We have also measured excitation cross sections of several other Fe L-shell transitions both at single electron impact energies [29, 32] and as a function of electron impact

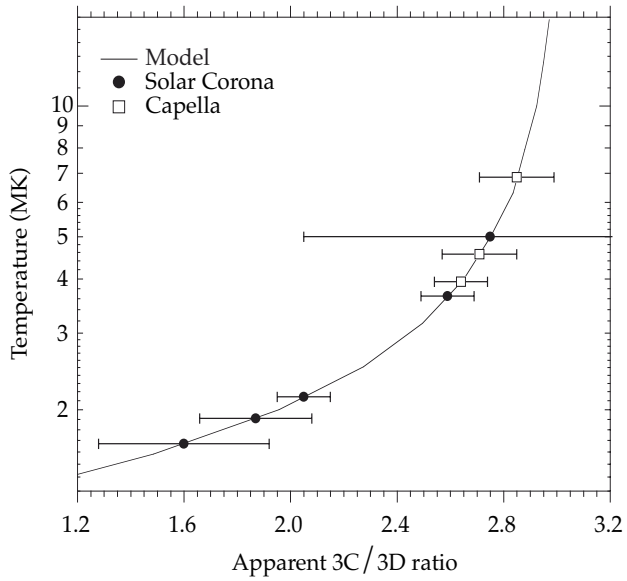

FIGURE 5. Correlation of the apparent I_{3C}/I_{3D} ratio with the electron temperature. This curve is from [23].

energy [33, 34]. Figure 6 shows the results of one of these measurements. In this case, the Fe XXIV line Li3 was measured as a function of electron energy by sweeping the beam energy linearly from an energy below the threshold for direct excitation to above threshold and recording the spectrum as function of energy. Once complete, the energy function is then absolutely calibrated by the cross section measured with the calorimeter at one or more single-electron beam energies. We note that this excitation function includes all relevant atomic processes that contribute to the line strength as a function of electron impact energy in collisional plasmas, including dielectronic recombination and resonance excitation. Therefore, this function can be integrated over any electron energy distribution and provide the proper rate coefficient and line strength.

DENSITY DIAGNOSTICS

In addition to temperature and opacity diagnostics, Fe L-shell transitions can provide a diagnostic of electron density. One example is the magnetic dipole line M2 in Fe XVII located at 17.096 Å. This transitions has a long lifetime and, in the case of high density plasmas can be collisionally de-excited. An example case where the absence of line M2 provides a lower limit on the electron density is given by Mauche et al. 2001 [35]. Recent studies also show a less well-known density diagnostic from boron-like Fe XXII [36]. In this case, in contrast to a long lived state being collisionally de-populated, a virtual ground state is populated collisionally from the true ground state. Once populated, collisional excitation from metastable ground state can significantly enhance the line strength of some x-ray lines. Figure 7 shows this density dependence in boron-like Fe XXII. Plotted is the ratio $R = (I_{3d_{5/2}\rightarrow 2p_{3/2}} + I_{3d_{3/2}\rightarrow 2p_{3/2}})/I_{3d_{3/2}\rightarrow 2p_{1/2}}$

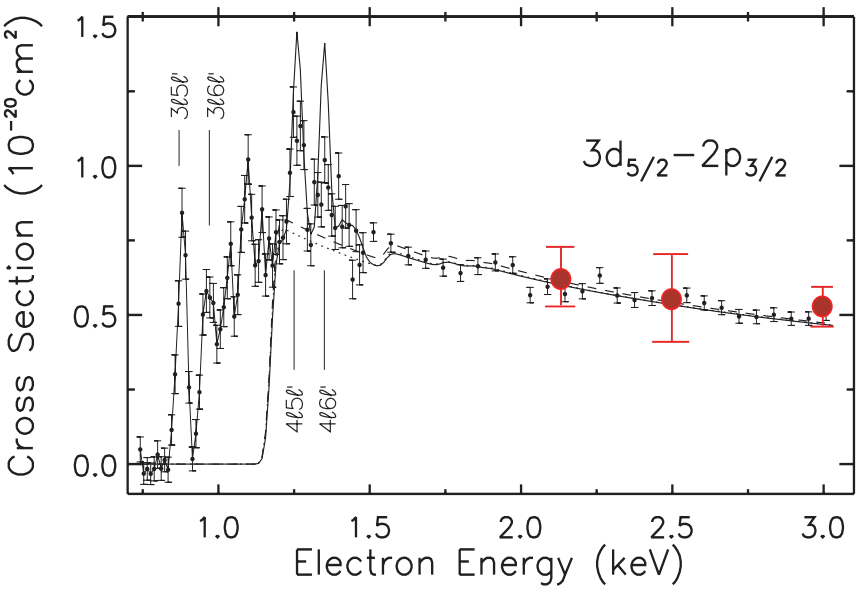

FIGURE 6. Excitation function of the Li-like Fe XXIV x-ray transitions. By measuring the line strength as a function of electron impact energy and by measuring its absolute cross sections, the excitation function of this line has been measured and absolutely calibrated in the laboratory. The large dots represent the absolute cross section measurements. This figure is from [34].

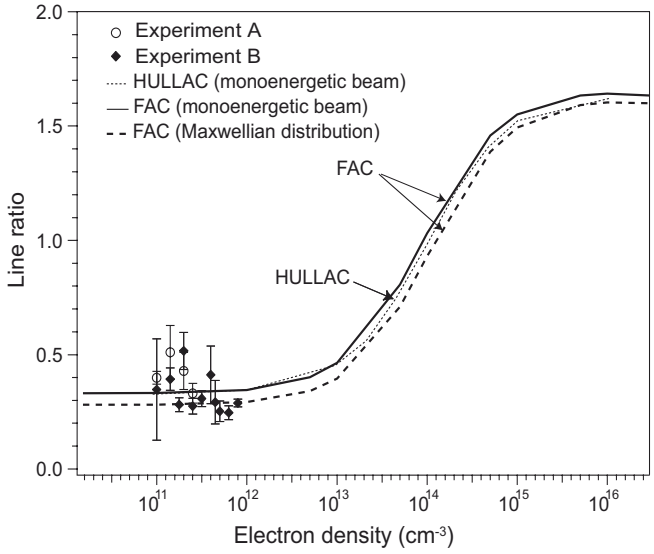

FIGURE 7. Ratio of $R = (I_{3d_{5/2}\to 2p_{3/2}} + I_{3d_{3/2}\to 2p_{3/2}})/I_{3d_{3/2}\to 2p_{1/2}}$ versus density. Two independent measurements are presented, labelled experiment A and experiment B. The experimental results are compared to calulcations from HULLAC and FAC. This figure is from [36].

versus density. These results are compared to calculations using HULLAC and FAC. The comparison shows good agreement between both theories and experiment. For a more detailed description of this result see Chen et al. [36].

SUMMARY

Laboratory astrophysics experiments in the study of Fe L-shell emission have provided accurate, complete sets of wavelengths, and several relative line intensities and absolute cross sections necessary for proper interpretation of astrophysical x-ray spectra. Future work includes measurement of the absolute excitation functions of all the significant Fe L-shell x-ray transitions, and extending our wavelength survey to below 10 Å. We have also extended our measurements to L-shell transitions from other ions where similar diagnostics exist. These include nickel [37], argon, sulfur [38, 39], and silicon. Experimental results such as the ones presented here provide quantitative error bars that can be used to estimate the accuracy of the physical parameters inferred from high-resolution spectra of astrophysical sources.

ACKNOWLEDGMENTS

Work at LLNL was completed under the auspices of the U.S. D.o.E by the University of California Lawrence Livermore National Laboratory under contract W-7405-Eng-48 and supported by NASA's Astronomy and Physics Research and Analysis Program under work order S-06553-G.

REFERENCES

1. Blake, R. L., Chubb, T. A., Friedman, H., and Unizicker, A. E., *Astrophys. J.*, **142**, 1 (1965).
2. Freeman, F. F., and Jones, B. B., *Solar Physics*, **15**, 288 (1970).
3. Parkinson, J. H., *Astron. Astrophys.*, **24**, 215 (1973).
4. Parkinson, J. H., *Solar Physics*, **42**, 183 (1975).
5. Hutcheon, R. H., Pye, F. P., and Evans, K. D., *Mon. Not. R. astr. Soc.*, **175**, 489 (1976).
6. McKenzie, D. L., Landecker, P. B., Broussard, R. M., Rugge, H. R., and Young, R. M., *Astrophys. J.*, **241**, 409 (1980).
7. Phillips, K. J. H., Leibacher, J. W., Wolfson, C. J., Parkinson, J. H., Kent, B. J., Mason, H. E., Acton, L. W., Culhane, J. L., and Gabriel, A. H., *Astrophys. J.*, **256**, 774–787 (1982).
8. Beiersdorfer, P., von Goeler, S., Bitter, M., and Thorn, D. B., *Phys. Rev. A*, **64**, 032705 (2001).
9. Von Goeler, S., Bitter, M., Cohen, S., Eames, D., Hill, K., Hillis, D., Hulse, R., Lenner, G., Manos, D., Roney, P., Roney, W., Sauthoff, N., Sesnic, S., Stodiek, W., Tenney, F., and Timberlake, J., "X-Ray Spectroscopy on Tokamaks," in *Diagnostics for Fusion Reactor Conditions*, edited by P. Scott., Commission of the European Communities, Belgium, 1982, p. 109.
10. Beiersdorfer, P., *Astron. Astrophys. Review*, **41**, 343–390 (2003).
11. McKenzie, D. L., and Landecker, P. B., *Astrophys. J.*, **254**, 309–317 (1982).
12. Boiko, V. A., Faenov, A. Y., and Pikuz, S. A., *J. Quant. Spectrosc. Radiat. Transfer*, **19**, 11–50 (1978).
13. Kelly, R. R., *J. Phys. Chem. Ref. Data*, **16**, 861–873 (1987), supplement Series.
14. Mewe, R., Gronenschild, E. H. B. M., and van den Oord, G. H. J., *Astron. Astrophys. Supp.*, **62**, 197–254 (1985).
15. Mewe, R., and Gronenschild, E. H. B. M., *Astron. Astrophys. Supp.*, **45**, 11–52 (1981).
16. Brown, G. V., Beiersdorfer, P., Kahn, S. M., Liedahl, D. A., and Widmann, K., *Astrophys. J.*, **502**, 1015–1026 (1998).
17. Brown, G. V., Beiersdorfer, P., Liedahl, D. A., Widmann, K., and amd E. J. Clothiaux, S. M. K., *Astrophys. J. Supp.*, **140**, 589–607 (2002).
18. Drake, J. J., Swartz, D. A., Beiersdorfer, P., Brown, G. V., and Kahn, S. M., *Astrophys. J.*, **521**, 839–843 (1999).
19. Ness, J., Brickhouse, N. S., Drake, J., and Huenmoerder, D. P., *Astrophys. J.*, **598**, 1277–1289 (2003).

20. Behar, E., Cottam, J., and Kahn, S. M., *Astrophys. J.*, **548**, 966–975 (2001).
21. Xu, H., Kahn, S. M., Peterson, J. R., Behar, E., Paerls, F. B. S., Mushotzky, R. F., Jernigan, J. G., and Makishima, K., *Astrophys. J.*, **579**, 600 (2002).
22. Waljeski, K., Moses, D., Dere, K., Saba, J. L. R., Web, D. F., and Zarro, D. M., *Astrophys. J.*, **429**, 909–923 (1994).
23. Brown, G. V., Beiersdorfer, P., Chen, H., Chen, M. H., and Reed, K. J., *Astrophys. J. Lett.*, **557**, L75–L78 (2001).
24. Arnaud, M., and Raymond, J., *Astrophys. J.*, **398**, 394–406 (1992).
25. Porter, F. S., Beiersdorfer, P., Boyce, K. R., Brown, G. V., Chen, H., Kelley, R. L., and Kilbourne, C. A., *Rev. Sci. Instrum.* (2004), in press.
26. Porter, F. S., Beiersdorfer, P., Boyce, K. R., Brown, G. V., Chen, H., Gendreau, K. C., Gygax, J., Kahn, S. M., Kelley, R. L., Liedahl, D. A., Stahl, C. K., Szymkowiak, A. E., and Widmann, K., p. 184 (2001).
27. Porter, F. S., Audley, M. D., Beiersdorfer, P., Boyce, K. R., Brekosky, R. P., Brown, G. V., Gendreau, K. C., Gygax, J., Kahn, S. M., Kelley, R. L., Stahle, C. K., and Szymkowiak, A. E., "Laboratory Astrophysics using a Spare XRS Microcalorimeter," in *Proceedings of the 45th annual SPIE meeting on Optical Science and Technology*, SPIE Press, 2000, p. 4140.
28. Brown, G. V., Beiersdorfer, P., Chen, H., Scofield, K., Boyce, K. R., Kelley, R. L., Kilbourne, C. A., Porter, F. S., Szymkowiak, A. E., and Kahn, S. M. (2004).
29. Chen, H., Beiersdorfer, P., Brown, G. V., Gendreau, K. C., Boyce, K. R., Kelley, R. L., Porter, F. S., k. Stahle, C., Szymkowiak, A. E., Kahn, S. M., and Scofield, J., *Astrophys. J. Lett.*, **567**, L169–L172 (2002).
30. Beiersdorfer, P., Bitter, M., and von Goeler, S., *Astrophys. J.*, **610**, 616–623 (2004).
31. Beiersdorfer, P., Behar, E., Boyce, K. R., Brown, G. V., Chen, H., gendreau, K. C., Gu, M.-F., Gygax, J., Kahn, S. M., Kelley, R. L., Porter, F. S., Stahle, C. K., and Szymkowiak, A. E., *Astrophys. J. Lett.*, **576**, L169–172 (2002).
32. Chen, H., Beiersdorfer, P., Scofield, J. H., Brown, G. V., Boyce, K. R., Kelley, R. L., Kilbourne, C. A., Porter, F. S., Gu, M. F., and Kahn, S. M., *Astrophys. J.* (2004), accepted.
33. Gu, M. F., Beiersdorfer, P., Brown, G. V., Kahn, S. M., Liedahl, D. A., Reed, K. J., and Savin, D. W., *Astrophys. J.*, **563** (2001), dec.
34. Gu, M. F., Kahn, S. M., Savin, D. W., Behar, E., Beiersdorfer, P., Brown, G. V., Liedahl, D. A., and Reed, K. J., *Astrophys. J.*, **518**, 1002 (1999).
35. Mauche, C. W., Liedahl, D. A., and Fournier, K. B., *Astrophys. J.*, **560**, 992–996 (2001).
36. Chen, H., Beiersdorfer, P., Heeter, L. A., Liedahl, D. A., Naranio-Rivera, K. L., Trabert, E., Gu, M. F., and Lepson, J. K., *Astrophys. J.*, **611**, 598 (2004).
37. Gu, M. F., Beiersdorfer, P., Brown, G. V., Chen H., Boyce, K. R., Kilbourne, C. K., Porter, F. S., Kahn, and S. M., *Astrophys. J. Lett.*, **607**, L143 (2004).
38. Lepson, J. K., Beiersdorfer, P., Behar. E., and Kahn, S. M., *Astrophys. J.*, submitted (2005).
39. Lepson, J. K., Beiersdorfer, P., Brown, G. V., Kahn, S. M., Liedahl, D. A., Mauche, C. W., and Utter, S. B. *Proceedings of the NASA Laboratory Astrophysics Workshop*, (2002).